

RESEARCH

Open Access



Green lithium: photoelectrochemical extraction

Zhongxiao Li^{1†}, Zhen Li^{2†}, Hao Huang^{2,3†}, Yunduo Yao⁴, Bilawal Khan¹, Ye Zhu⁴, Kuo-Wei Huang^{2,3,5*}, Zhiping Lai^{2*} and Jr-Hau He^{1*}

[†]Zhongxiao Li, Zhen Li and Hao Huang contributed equally to this work.

*Correspondence: kuowei.huang@kaust.edu.sa; zhiping.lai@kaust.edu.sa; jrheu@cityu.edu.hk

¹ Department of Materials Science and Engineering, City University of Hong Kong, Kowloon, Hong Kong SAR 999077, China

² Division of Physical Science and Engineering, King Abdullah University of Science and Technology (KAUST), Thuwal 23955-6900, Saudi Arabia

³ KAUST Catalysis Center, King Abdullah University of Science and Technology (KAUST), Thuwal 23955-6900, Saudi Arabia

⁴ Department of Applied Physics, Research Institute for Smart Energy, The Hong Kong Polytechnic University, Kowloon, Hong Kong SAR 999077, China

⁵ Agency for Science, Technology, and Research, Institute of Materials Research and Engineering and Institute of Sustainability for Chemicals, Energy and Environment, Singapore 138634, Singapore

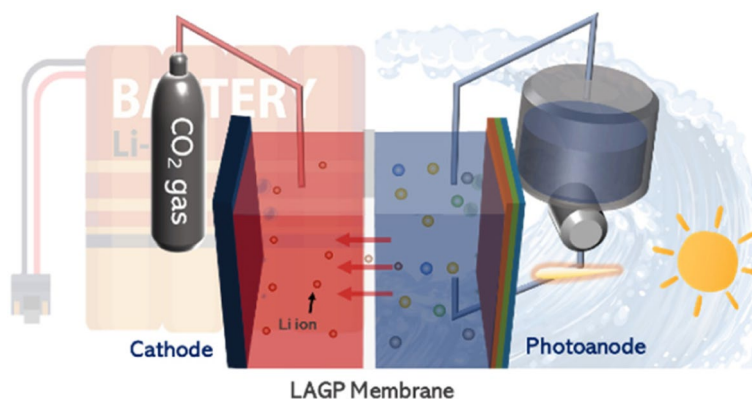
Abstract

Lithium (Li) is an essential element in modern energy production and storage devices. Technology to extract Li from seawater, which contains ~ 230 billion tons of Li, offers a solution to the widespread concern regarding quantitative and geographical limitations of future Li supplies. To obtain green Li from seawater, we propose an unassisted photoelectrochemical (PEC) Li extraction system based on an III-V-based triple-junction (3J) photoelectrode and a Li-ion selective membrane with only sunlight as an input. A light-harvesting/catalysis decoupling scheme yielded a 3J photoelectrode with excellent light-harvesting and catalysis reaction capabilities and superb stability over the 840 h of the extraction process. It allows the system to successfully enrich seawater Li by 4,350 times (*i.e.*, from 0.18 ppm to 783.56 ppm) after three extraction stages. The overall reaction of the unassisted PEC green Li extraction system achieved 2.08 mg kJ⁻¹ of solar-to-Li efficiency and 3.65% of solar-to-hydrogen efficiency.

Keywords: Photoelectrochemical, Unassisted Li extraction, Seawater, Green Li

Graphical Abstract

Photoelectrochemical (PEC) lithium extraction device is designed to explore lithium from seawater for the first time. The PEC cell with a triple-junction (InGaP/GaAs/Ge) photoelectrode and light-harvesting/catalysis decoupling scheme is constructed, offering a suitable operating potential and superb stability to the membrane-based extraction process in the seawater. The device can successfully enrich lithium by 4,350 times (from 0.18 to 783.56 ppm).



Introduction

Since lithium (Li) has rapidly emerged as a strategically important resource [1–4], the future security of Li supply has raised concerns throughout the energy sector. One-quarter of global lithium reserves will be consumed by electric vehicles alone before 2050 [5, 6]. Besides, the geographic distribution of land-based Li is highly uneven. The traditional Li exploitation methods involve a long time and large quantities of reagents, leading to cost increases and environmental pollution [7]. Fortunately, the ocean as a Li-rich source, containing four orders of magnitude larger (~230 billion tons) than the Li reserves on land and overcoming location-dependent limitations, provides an option for most countries to explore Li resources infinitely and directly. Despite far lower concentrations of Li (0.1–0.2 ppm) in seawater than other ions, all of which are over 13,000 ppm, various innovative strategies have demonstrated the feasibility of extracting Li directly from seawater [6, 8–12]. The ceramic-based membrane extraction process has been proved as a novel and promising technique with high selectivity and continuity. However, current technologies do not eliminate the reliance on fossil fuels, still facing energy shortage problems and environmental pollution issues.

The goal of carbon neutrality forces green energy and resource, like 'green hydrogen,' to become the central theme in the energy sector [13–15]. Similarly, 'green Li'—extracted from an inexhaustible resource using only renewable energy as an input—will be the 'final answer' for the sustainability of Li-based industries. Solar energy is one of the most promising energy sources for the green Li extraction process as it is inexhaustible and environmentally friendly. Photoelectrochemical (PEC) cells, which combine light-harvesting and electrochemical processes to directly store solar energy in chemical bonds, offer the possibility of eliminating external wiring and minimizing reliance on electrolyzers [16–18]. The integrated systems also provide an opportunity to implement thermal management, wherein the aqueous electrolyte solution cools the illuminated semiconductor,

maintaining a high photovoltage. In contrast, the electrocatalyst/solution is heated, lowering the overpotential. PEC devices have been regarded as a promising platform that provides a competitive and economical solution for medium- and long-term solar energy utilization [19–21]. Therefore, combining PEC and Li-ion selective membrane technologies offers a feasible strategy to achieve consecutive green Li extraction.

Tremendous efforts have been undertaken to design and develop feasible unassisted PEC cells that can efficiently perform various PEC reactions driven by sufficient photovoltage and use only sunlight as energy input [22–24]. However, the membrane extraction process always involved the electrochemical redox reactions on both electrodes and the migration of Li ions in the membrane, which required high applied voltage (over 2 V) to drive the operation [25–28]. To construct an unassisted PEC Li extraction device, an III-V-based (InGaP/GaAs/Ge) triple-junction (3J) photoanode with an open-circuit potential (V_{oc}) of 2.47 V was designed. Moreover, the longtime stability of PEC operation in the seawater was another big concern for the final application [29–34], as the nature of poor photo-corrosion resistance of III-V semiconductors [35] and the corrosive chlorine gas producing near photoanode. Therefore, an innovative decoupled scheme of PEC cell was proposed, which allows the light-harvesting (front) side to be covered by a low-cost soda-lime glass as a transparent protective layer and the electrolysis (back) side protected by a potent Ti layer. The decoupled scheme provides the photoanode with excellent stability > 840 h for extraction process conditions. Combining the decoupled scheme 3J PEC cell and Li-ion selective membrane, we successfully extracted the high-purity green Li from seawater for the first time while storing solar energy as hydrogen energy with high efficiency. The PEC technology for green Li mining drives real progress across a broad range of technological designs and manufacturing areas, which have presented inspiring results and may break the status quo of Li supply.

Results and discussion

Decoupling design for III-V-based triple-junction PEC cells

Light-harvesting ability, electrolysis, and stability of the device are the main factors that must be carefully adjusted in traditional monofacial PEC device configuration. This is attributed to the fact that all major components of the device are mainly integrated on the illuminated side of the device that is illuminated (Figure S1a). The light reflection and parasitic absorption of opaque catalyst layer (R_c and A_c), along with the protection layer (R_p and A_p), substantially block the light arriving at the photo-absorber. This limits the photocurrent in monofacial PEC devices. In contrast, an innovative scheme was used in our proposed device for Li extraction that decouples the optical absorption and electrocatalytic interfaces (Fig. 1a and S1b). Moving the catalyst and protection layer to the back of the device avoids the wastage of light that may be caused by the shadowing effect of co-catalysts or gas products before it reaches the photo-absorber. In addition, a thick layer of titanium (Ti) foils ($\sim 200 \mu\text{m}$) was employed as a protective layer and co-catalyst supporter to yield a PEC cell with excellent stability during the seawater Li extraction process (as discussed in the "Stability of the PEC green Li extraction device" section).

The composition and structure of the photo-absorber in the proposed PEC cell were revealed using high-angle annular dark-field scanning transmission electron microscopy (HAADF-STEM) with elementary distribution mapping. As shown in Fig. 1b, the composites of the top, middle, and bottom cells included InGaP, GaAs,

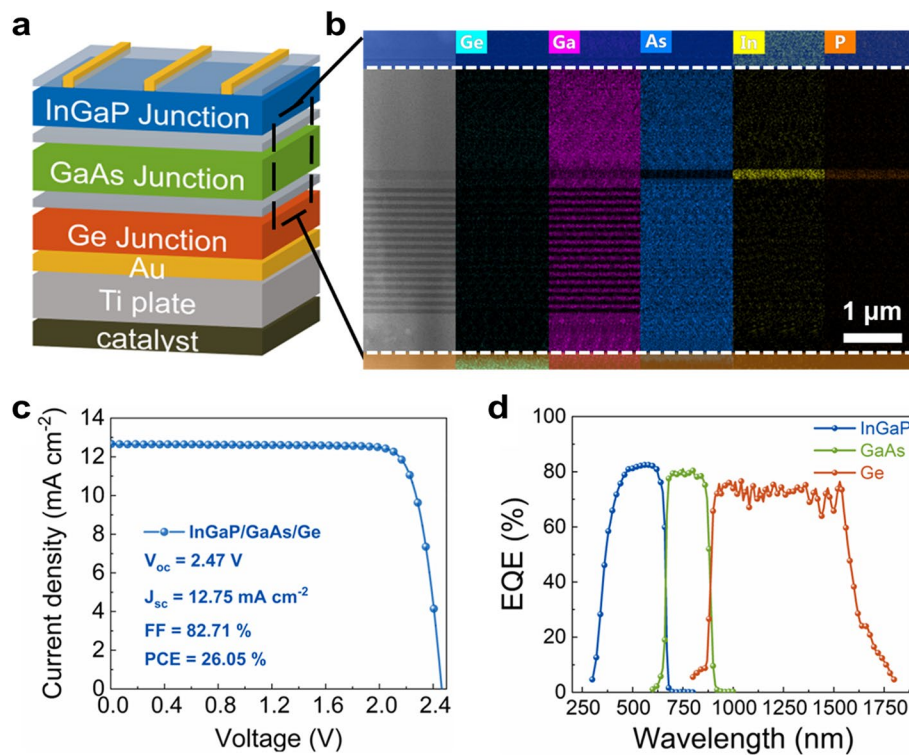


Fig. 1 **a** Schematic representation of spatially and functionally decoupled III-V-based 3J photoanode. **b** HAADF-STEM image of photo-absorber of PEC cell and the corresponding elemental mapping images. **c** J-V characteristics of the InGaP/GaAs/Ge 3J cell under 1 sun AM 1.5G illumination. **d** EQE measurement of the InGaP/GaAs/Ge 3J cell

and Ge, respectively. Two highly doped wide bandgap materials were deposited as a tunnel junction connecting the subcells in series to construct the 3j photo-absorber for the PEC cell. Thus, the photovoltages of three subcells in the 3j PEC cell will be added during illumination, and therefore the V_{oc} achieved is higher than the potential required to drive unassisted Li extraction. In addition, multiple quantum wells were introduced in the middle cell (GaAs junction) to broaden the absorption spectrum. To quantitatively identify the V_{oc} and the light-harvesting ability, the PV characteristics of the III-V-based 3J cells, which consist of top (InGaP, $E_g = 1.80$ – 1.85 eV), middle (GaAs, $E_g = 1.40$ eV), and bottom subcells (Ge, $E_g = 0.67$ eV) were measured under AM 1.5 G simulated one-sun conditions. As shown in Fig. 1c, the V_{oc} , short-circuit current density (J_{sc}), fill factor (FF), and power conversion efficiency were 2.47 V, 12.75 mA cm^{-2} , 82.71%, and 26.05%, respectively. In addition, the external quantum efficiency (EQE) of the solid-state device was characterized (Fig. 1d). First, the GaInP top subcell absorbed almost all photons with a wavelength of 300–600 nm. After that, the photons that passed through the top cell entered the GaAs middle subcell region, where photons of wavelength 600–900 nm were absorbed. Finally, the remaining photons of wavelength 900–1,800 nm were absorbed by the Ge bottom subcell. These results highlight high photovoltage and excellent light absorption of the III-V-based 3J photoanode.

PEC green Li extract setup

A schematic of the PEC green Li extraction device designed in this study is shown in Fig. 2a. The device was divided into two compartments: the enrichment chamber (deionized water) on the cathode side and the feed chamber (seawater) on the anode side. Both chambers were separated by a dense crystalline ceramic membrane with a diameter of ~ 12 mm (Fig. 2b) and a thickness of $600\ \mu\text{m}$ (Figure S2). A type of solid-state Li-ion superconductor, $\text{Li}_{1.5}\text{Al}_{0.5}\text{Ge}_{1.5}(\text{PO}_4)_3$ (LAGP), was applied in this work. Due to its distinctive crystal structure, the LAGP membrane usually has a Li-ion conductivity one order of magnitude higher compared to the $\text{Li}_{0.33}\text{La}_{0.56}\text{TiO}_3$ (LLTO) membrane reported in our previous study [25], which is critical to achieving high Li^+ permeance. Besides, this dense membrane can also provide a high selectivity of Li ions and successfully preserve other disturbing ions (i.e., Na^+ , K^+ , Mg^{2+} , and Ca^{2+}) passing through (Figure S3) [6, 27, 28]. The obtained membrane was identified as LAGP using the X-ray diffraction (XRD) spectroscopy pattern (Figure S4). The III-V-based 3J photo-absorber was designed as a photoanode immersed in seawater. During the extraction process, an imbalance in the charge was caused as Li ions passed through the LAGP membrane from the feed chamber to the enrichment chamber driven by the 3J PEC cell. Hence, the excess Cl^- in the feed chamber needed to be directly consumed by the holes produced at the back side of the photoelectrode. Chlorine gas (Cl_2) was released via Reaction 1. Meanwhile, the electrons produced from the front side were collected by the interdigitated Au/Ti grid and transferred to the Pt electrode to consume the excess cations (H^+) in the enrichment chamber (Reaction 2). As the protons were continuously consumed, the pH in the enrichment chamber would increase, resulting in the corrosion of the LAGP membrane. Therefore, CO_2 was constantly introduced into the enrichment chamber during operation to buffer pH changes. In addition, CO_2 can be fixed via the formation of a super carbonate in the final enrichment solution.

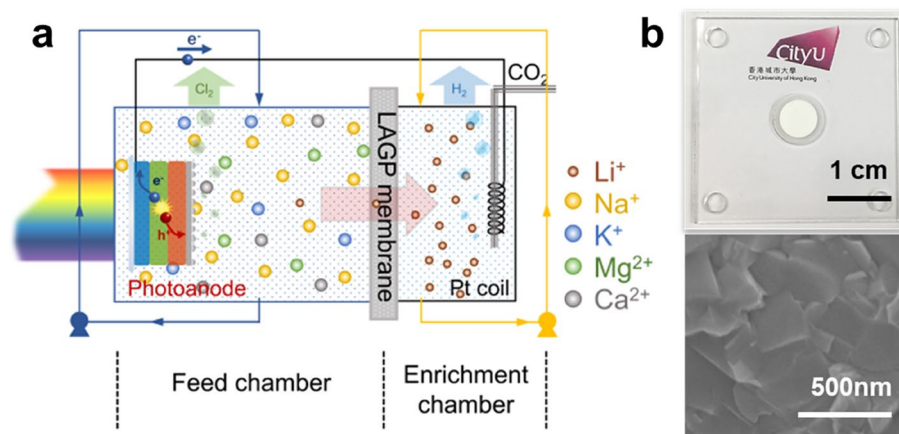
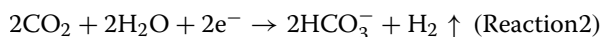


Fig. 2 **a** Schematic illustration of the two-compartment PEC device to continuously enrich Li from the feed solution to the cathode compartment and simultaneously generate H_2 and Cl_2 at the cathode and anode, respectively, under 1 sun AM 1.5G illumination. **b** The digital and high magnification SEM image of the surface of the LAGP membrane (~ 12 mm in diameter)

Anode:



Cathode:



PEC green Li extraction process test

This work deliberately implemented a three-stage extraction process (each stage lasts 20 h) to obtain a high-purity Li^+ solution in the final enrichment solution. This can, in turn, facilitate more accessibility to a solid-state Li product (as described at the end of this section), which is indeed the preferable form in the Li extraction industry. To intuitively reflect the results of the PEC Li extraction process, the detailed concentrations of the major ions in the seawater (Red Sea) and enrichment solutions after each stage were listed in Table 1. Only the concentration of Li-ion was continuously enriched, whereas those of other ions remained considerably low. In the 1st stage, the Red Sea water sample was circulated in the feed chamber, and deionized water was used as the initial enrichment solution. Under 20 h of illumination, the designed PEC Li extraction device continuously extracted the Li ions from seawater to the enrichment solution, eventually reaching a concentration of 37.07 ppm, which was 200 times higher than the original Li concentration in seawater. The PEC Li extraction device can also achieve a Li/Mg and Li/Na selectivity of ~16 million and ~0.5 million, respectively. The Li/M selectivity (M represents either Na^+ or Mg^{2+}) is an essential index that could reflect the Li ion-selective capacity and purity in the final enriched solution. The high Li/Mg selectivity implies the presence of fewer co-precipitated ions in the final solution allowing obtaining pure solid-state Li products for direct precipitation in one of the later steps. The high Li/Na selectivity presents fewer soluble ions, dramatically reducing the post-cleaning process of solid products. After three extraction stages, the III-V-based photoanode finally enriched Li^+ to 783.56 ppm with a lumped Li/Mg selectivity of over 50 million and a lumped Li/Na selectivity of over 1.9 million. Except for the Na ions and Mg ions, the PEC extraction process also exhibited good selectivities of other ions during the three extraction stages, all summarized in Table S1.

In addition, Fig. 3a presents the photocurrent of the device at each stage over time. The stable photocurrent indicated that all the main components in our device (the photoanode and LAGP membrane) were robust for at least 20 h at the working condition. The plot of steady-state current and Li feed concentration (Fig. 3b) shows that the current increased with the increase in Li^+ concentration in the feed solution,

Table 1 Concentration of the major ions in Red Sea water and enriched solutions

	Li (ppm)	Na (ppm)	K (ppm)	Mg (ppm)	Ca (ppm)
Seawater	0.18 ± 0.02	10,565.04 ± 97.86	665.56 ± 14.08	1610.81 ± 28.35	475.87 ± 4.48
1 st stage	37.07 ± 0.85	4.31 ± 0.04	0.33 ± 0.08	0.02 ± 0.01	0.15 ± 0.04
2 nd stage	265.09 ± 1.25	8.53 ± 0.05	2.91 ± 1.08	0.03 ± 0.04	0.02 ± 0.01
3 rd stage	783.56 ± 11.73	23.69 ± 0.15	23.39 ± 0.57	0.14 ± 0.01	0.03 ± 0.01

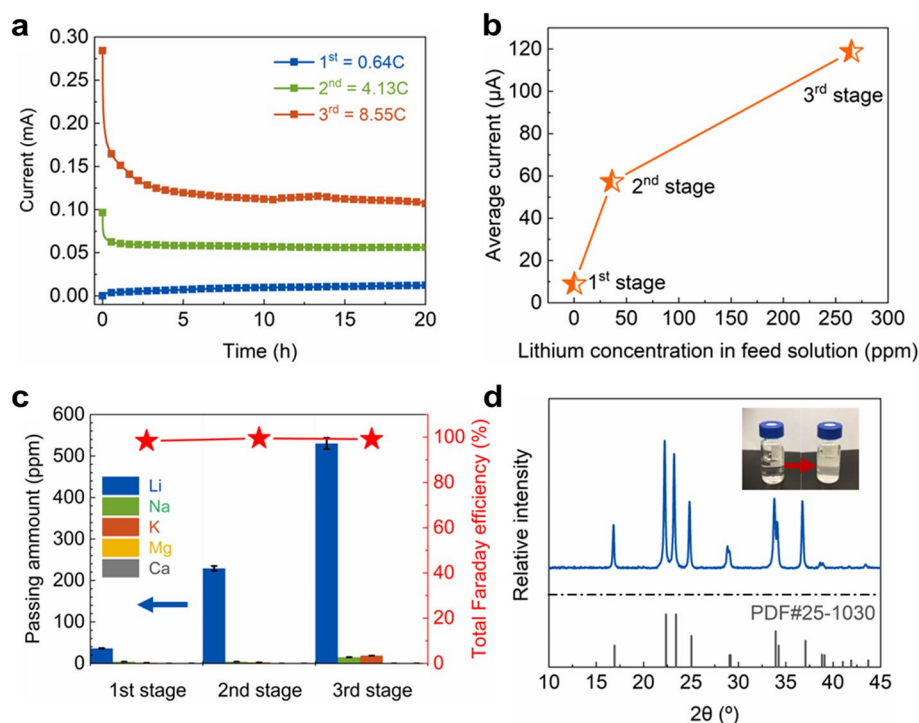


Fig. 3 **a** The chronoamperometric curve at each stage; integrating the area under the curve gives the total charge passing through the membrane in Coulombs for each stage. **b** The average photocurrent vs. the Li concentration in the feed solution at different stages. **c** The number of different ions passing through the membrane (bar chart) and the contributed faradaic efficiencies for each stage (red star). **d** The XRD pattern of the Li_3PO_4 sediment collected from enrichment solution after three extraction stages. The inset shows the enriched Li solution and the Li_3PO_4 sediment

demonstrating that the available Li^+ in the feed compartment primarily limited the entire photocurrent produced by the device. The Li-ion feed concentration was the lowest in the 1st stage, indicating that the 1st stage is the rate-determining stage of the entire extraction process. However, its extraction rate is determined to be $30.89 \text{ ug ppm}^{-1} \text{ cm}^{-1} \text{ h}^{-1}$, which still exhibits good performance compared to other extraction technologies, as shown in Table S2.

Figure 3c shows the concentration of ions in the enrichment chamber after each PEC extraction stage. In all three stages, the number of the major interfering ions (Na^+ , K^+ , Mg^{2+} , and Ca^{2+}) were negligible compared to Li ions. To further identify that the source of the Li extracted in the enrichment chamber is seawater, we evaluated the difference between the Li^+ amount before and after extraction (Δn_{feed}) in the feed chamber and the final amount ($n_{\text{enrichment}}$) in the enrichment chamber ("Methods" section). The result ($\Delta n_{\text{feed}} \approx n_{\text{enrichment}}$) demonstrated that almost all Li ions were directly extracted from the feed chamber, rather than the membrane dissolution (Figure S5). Besides, in the 20 h PEC seawater extraction process, the total Faradaic efficiencies of all stages, which represents the ratio of the total amount of charge brought to the charge integrated by the photocurrent produced by the PEC cell, were almost 100% (Fig. 3c). High Faradaic efficiency reflects that the ions in the enriched solution contribute to constructing the entire circuit. This verifies that the majority of the Li ions

were transported through the membrane, and Li^+ was successfully extracted from seawater. Furthermore, as there is no obvious change in the surface micromorphology of the membrane (Figure S6) and no new feature peaks appearing in the XRD spectra (Figure S4) after Li extraction process, the LAGP membrane presents good physical and chemical stability during the extraction process. After the three extraction stages, the solid-state Li product was directly precipitated at a concentration of ~ 800 ppm in the enriched solution (Fig. 3d, inset). The XRD spectra (Fig. 3d) of the final products fit well with the standard pattern of Li_3PO_4 (PDF#25–1030), demonstrating that high-purity solid-state Li products could be obtained from our PEC Li extraction device.

The PEC performance of the III-V-based 3J photoanode during the extraction process was characterized using a three-electrode configuration (Fig. 4a). As shown in Fig. 4b, the PEC chlorine evolution reaction (CIER) performance of the photoanode closely matched the PV performance of the device, with J_{Cl_2} and $|V_{\text{OS}} - E^0|$ of 12.45 mA cm^{-2} and 1.86 V vs. RHE, respectively (where J_{Cl_2} is the saturation current density at E^0 for CIER; V_{OS} is the onset potential measured at a photocurrent density of 1 mA cm^{-2} , and E^0 is the equilibrium chlorine ion oxidation potential). The fact that the value of J_{Cl_2} measured in the current study is similar to that of J_{sc} measured in the air can be attributed to: i) the neglectable series resistances caused by the excellent fabrication and integration of the PEC cells into the Li extraction systems and ii) the superior light absorption capability due to the decoupling of the light-harvesting and electrocatalysis components of the

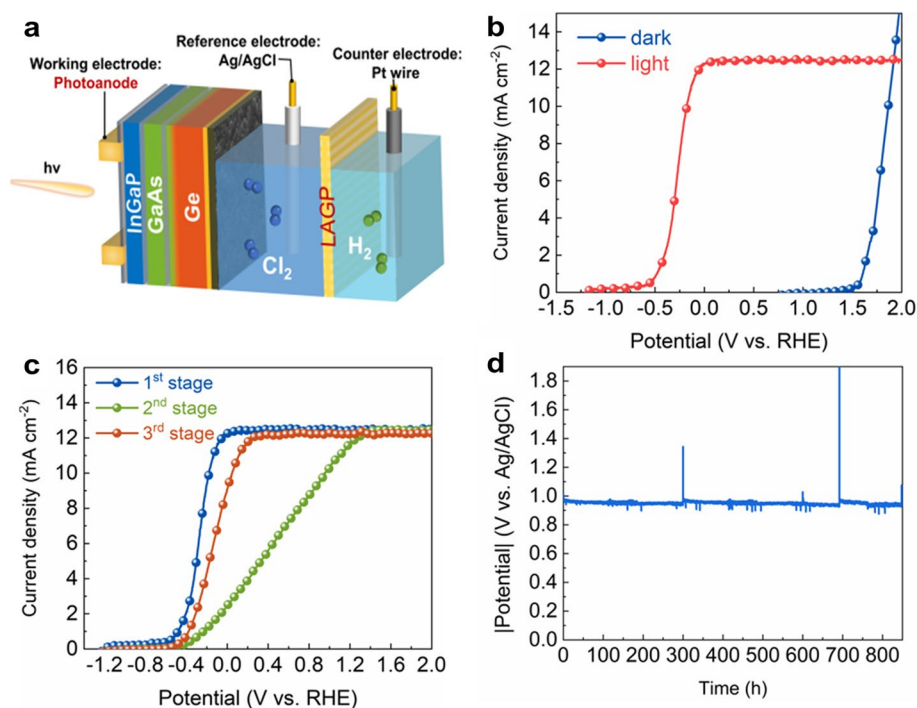


Fig. 4 **a** Schematic illustration of a three-electrode configuration for the PEC test. **b** LSV curves of the 3J photoanode measured in a three-electrode setup in Red Sea water (pH = 8.2) under 1 sun illumination and dark electrolysis of the Ru-Ir-TiO_x co-catalyst. **c** LSV curves of the photoanode under 1 sun illumination in a three-electrode setup for each extraction stage. **d** Chronopotentiometry experiments at a current density of 2.96 mA cm^{-2}

device. $|V_{OS} - E^0|$ reflected the potential that the photoanode can provide after overcoming the overpotential of the CIER. The difference (~ 0.6 V) between $|V_{OS} - E^0|$ and V_{oc} was mainly due to the high onset potential of the co-catalyst (~ 1.61 V), as shown in Fig. 4b. Integrating lower overpotential co-catalyst in PEC cell can be investigated to optimize this process further. Figure 4c compares the PEC performance of the photoanode at the three different extraction stages. The performance of the photoanode (onset potential and incremental photocurrent) exhibited the following trend: 1st stage > 3rd stage > 2nd stage, which presents the same trend as the Cl^- concentration in the electrolyte. However, it should be noted that the photocurrents of the entire system in the second and third stages (Fig. 3b) were higher than in the first stage. These results indicate that the performance of the whole system is determined by the Li^+ transportation process, which further proves the high Li-ion selectivity of the LAGP membrane.

Stability of the PEC green Li extraction device

Given that Cl_2 is corrosive and produced near the photoanode of PEC cells, the stability of PEC devices used in seawater is a major concern in real-world implementation [36]. In this work, more holes and Cl_2 were produced by the photoanode during the third stage as the highest photocurrent density. This implies that the photoanode is more likely to damage during the third stage than in the other two stages. Therefore, the stability of the photoanode in the third stage, which can reflect its actual stability performance, was carried out. Remarkably, the initial potential (vs. Ag/AgCl) of the photoanode was retained over 840 h of operation without any noticeable degradation (Fig. 4d). Figure S7 shows that the PEC stability demonstrated in the present study is better than those presented in previous studies as most PEC cells cannot work in seawater for more than 10 h [29–32, 34]. This excellent stability benefits from the decoupling PEC configuration, which allows a robust protection layer introduced in the system without compromising the light-harvesting efficiency.

PEC green Li extraction performance evaluation

Given the difficulties surrounding the calculation of stored energy within Li, we recommend evaluating the solar-to-Li extraction efficiency (η_{STLi}) by the Li quantity (mg) against the incident solar energy (kJ), which can be derived using Eq. (1):

$$\eta_{STLi} \left(mgkJ^{-1} \right) = \frac{J_{Li} / (nF) \times M_{Li}}{P_{in}} \times 10^6 \quad (1)$$

where J_{Li} is the average current density for PEC Li extraction caused by Li^+ transportation ($mA\ cm^{-2}$), which is the product of the total current in the system and the Faradaic efficiency of Li ions for each stage (Fig. 5a); n is the valence state of the Li-ion (+1); F is the Faradaic constant ($96,485\ C\ mol^{-1}$); M_{Li} is the atomic weight of Li ($6.941\ g\ mol^{-1}$), and P_{in} is the incident optical power illuminating the PEC cell surface ($100\ mW\ cm^{-2}$).

Figure 5b shows the J_{Li} and η_{STLi} for each PEC Li extraction stage. In the first stage, J_{Li} was $0.21\ mA\ cm^{-2}$. In comparison, J_{Li} reached $1.42\ mA\ cm^{-2}$ and $2.92\ mA\ cm^{-2}$ in the second and third stages, respectively. The η_{STLi} improved from 0.15 to

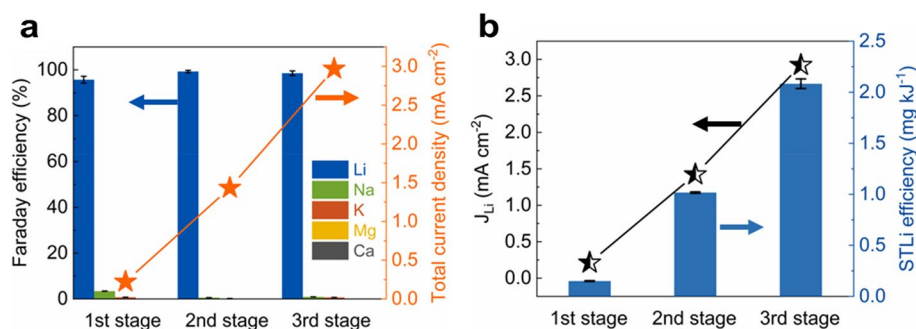


Fig. 5 **a** The contributed faradaic efficiencies of the different ions (bar chart) and the total current density (orange line) for each stage. **b** The averaged current density converted to Li-ion extraction (J_{Li} , black line) and the corresponding solar-to-Li extraction efficiency (η_{STLi}) for each stage (blue bar)

1.01 mg kJ⁻¹ in the second stage and finally reached 2.08 mg kJ⁻¹ in the third stage. Hydrogen molecules were also produced in the enrichment chamber when Li was extracted. The solar-to-hydrogen efficiency (η_{STH}) was calculated for the three extraction stages using Eq. (2) [13]:

$$\eta_{STH}(\%) = \frac{\text{Rate of } H_2 \text{ production} \times \Delta G_{H_2+O_2=H_2O}}{P_{in}} \times 100 = \frac{J \times 1.23V}{P_{in}} \times 100 \quad (2)$$

where J is the total current density for PEC Li extraction caused by all ion transportation (mA cm⁻², Fig. 5a). In the first stage, J was 0.22 mA cm⁻². It can reach 1.43 and 2.96 mA cm⁻² in the second and third stages, respectively (Figure S8). Correspondingly, the η_{STH} improved from 0.27 to 3.65%.

The first stage was the rate-determining stage of the PEC Li extraction process, but even with its η_{STLi} of 0.15 mg kJ⁻¹, ~12.0 kg of Li, which is roughly required by an electric vehicle, could be extracted from seawater by our system within a day (an 8 h 1-sun illumination per day) with a 2,800 m² or roughly 2/5 football field size PEC device. At the same time, this PEC system can also produce ~1.5 kg H₂ and fix ~76.7 kg CO₂ in the form of bicarbonate in the final enrichment solution. Although the value of the solar energy conversion efficiency was not comparable to the highest efficiency of the PEC water splitting/CO₂ reduction [37, 38], the total economic value produced by our system is as high as ~US\$ 1.7 m⁻² per day, especially with the high value of Li products (cost of Li₂CO₃ = ~US\$ 75.0 kg⁻¹). This remarkable economic value indicates the future potential of this PEC Li extraction method. The major challenge of the proposed system is associated with the feasibility of scaling up the process while maintaining stable performance, especially for the Li-ion selective membrane. Although the membrane exhibits high Li selectivity performance, the presence of tiny cracks can result in leakage of other ions, which can substantially impact the stability of the membrane. In addition, a long operation time (over 20 h) may result in Li⁺ leaching from the membrane, which is highly dependent on the fabrication process. Hence, the stability of the membrane should

be accurately evaluated and improved in the future. Moreover, the mechanism of the entire extraction process should be identified to ensure the practical use of this Li extraction system.

Conclusions

Green Li extracted from an inexhaustible source using renewable energy provides a promising solution to the present Li resource crisis and environmental issues. In the present study, we proposed and implemented a system for green Li extraction from seawater using an unassisted III-V-based 3J PEC cell and Li-ion selective membrane for the first time. A decoupling scheme was employed on the PEC cell design, which provided excellent stability for >840 h of active operation. The system can successfully enrich Li through a three-stage extraction process from the base seawater concentration of 0.18 ppm to 783.56 ppm with negligible impurities. Currently, the final η_{STLi} and η_{STH} of the PEC system reached up to 2.08 mg kJ^{-1} and 3.65%, even when the initial efficiency at the first stage was 0.15 mg kJ^{-1} and 0.27%, respectively. In addition, our PEC Li extraction system may have huge potential to recovery Li from spent Li-ion batteries, as spent Li-ion batteries can be regarded as an enormous Li resource with higher Li contents compared to seawater [39–42]. To further optimize the proposed system, a highly active co-catalyst should be integrated, the fabrication process for high stability and Li-ion conductivity membrane should be optimized, and a more compact device configuration should be explored. As global attention is focused on lowering carbon emissions and struggling with a lack of reliable Li supplies, green Li extraction will be critical for the energy storage system. The finding of our present study represents a significant milestone for establishing circular and zero-carbon economies.

Methods

Mixed metal oxide (Ru-Ir-TiO_x) electrode synthesis

To obtain good catalytic performance of the oxidation reaction and ensure its stability in seawater, a mixed metal oxide catalyst (Ru-Ir-TiO_x) for the chlorine evolution reaction (CIER) was fabricated. A thermal treatment method was used to synthesize the electrode; this method yielded an electrode with compact morphology featuring mud cracks (Figure S9) [43]. The dimensionally stable electrode was prepared as previously described. Briefly, a Ti plate (thickness ~200 μm) was cleaned by sonication in acetone and then etched as the substrate using 10% boiling oxalic acid solution for 2 h. A paint solution (Ru:Ir:Ti of molar ratio 25:25:50) was prepared by dissolving ruthenium(III)-hydrated chloride (99.98% trace metals basis, Sigma-Aldrich), iridium(III)-hydrated chloride (99.9% trace metals basis, Sigma-Aldrich), and titanium diisopropoxide bis-2,4-pentanedionate (75% isopropanol solution, Thermo Scientific™). This paint solution was applied to the pretreated Ti substrate using a brush. Thereafter, the sample was dried at 90 °C for 10 min in an oven and then sintered in a furnace at 450 °C for 10 min. The operation was repeated until the nominal thickness of the electrode was ~10 μm. The electrode was finally annealed at 450 °C for 1 h.

PEC cell fabrication

The Ga-In eutectic was applied on the top finger electrode to ensure Ohmic contact without shorting the PEC device. A thin foil contact lead of Cu was taken out using the protection of a high-grade polystyrene pipette tip. Thereafter, a thin quartz slide was used to cover the top side of the III-V triple-junction (3J) cell. For the electrocatalytic (back) side of the cell, a thin gold (Au) layer was used to ensure Ohmic contact by Fermi level pinning near the valence band edge of Ge [44]. This further reduces the losses of minority carrier recombination in Ge substrates and reflects back the unabsorbed photons with long wavelengths for reabsorption. Subsequently, the Ru-Ir-TiO_x electrode was attached to the Au layer using silver paste. The sample was finally embedded in Epoxy (Hysol 1C) such that only the part covered by mixed metal oxide catalyst was exposed to the electrolyte.

LAGP membrane fabrication

LAGP membrane was prepared using a solid-state reaction method. First, 18.60 g Li₂CO₃ (ACS reagent, >99.0%, Sigma-Aldrich), 8.157 g Al₂O₃ (particle size <50 nm, Sigma-Aldrich), and 50.23 g GeO₂ (>99.99% trace metals basis, Sigma-Aldrich) were dispersed in 200 mL of isopropanol. Subsequently, 110.04 g NH₄H₂PO₄ (99.5%, Sigma-Aldrich) was added to the suspension by stirring. The mixture was then blended further using a ball grinder, and thereafter, it was dried at 80 °C, sintered at 600 °C for 4 h, and then sintered again at 900 °C for 6 h under air at heating and cooling rates of 2 °C min⁻¹. The resulting white LAGP powder was ball-milled at 300 rpm for 12 h to obtain LAGP nanoparticles. After that, the LAGP nanoparticles were loaded into a Tungsten carbide pellet mold and pressed into disks to form the green bodies of the membranes, with diameters of 12 mm. The green bodies were sintered in a high-temperature furnace at 600 °C for 2 h and then at 880 °C for 8 h to produce the LAGP membranes. The heating and cooling rates of the sintering process were 2 °C min⁻¹.

Unassisted photoelectrochemical Li extraction process

The PEC Li extraction process was performed in a customized H-shaped cell separated by a LAGP membrane at 25 °C. The III-V-based photoelectrode was used as the anode on the feed side, whereas a Pt coil electrode was used as the cathode immersed in the DI water saturated with CO₂ gas on the enrichment side. In the system used in the present study, the light-harvesting side was illuminated through a thin quartz window. In contrast, the catalyst layer was in contact with the electrolyte at the location where the CIER proceeded. The process was measured on a BioLogic VMP3 potentiostat at 25 °C using the standard two-electrode setup under chronoamperometric conditions without any bias. A 150 W halogen-lamp-based solar simulator (Newport Corporation, AAA Class) with Air Mass 1.5 Global (AM 1.5 G) solar filters was calibrated to 100 mW cm⁻² (1 sun) using a certified standard power meter (RQN3724, ABET Inc.). The ions concentration of the enriched solution after 20 h extraction process was analyzed by ICP-OES. All the samples were tested three times to reduce the random error. The seawater sample was fetched from the Red Sea with location around 21°27'N 38°54'E. The water sample

was filtered using fine filter papers (Whatman acid-treated and low metal grade, Sigma-Aldrich) and then used without further treatment. During the extraction process, the solution volume circulated on the feed side was 25 L for the first stage and 2.5 L for the remaining two stages, whereas the solution volumes at the cathode were fixed at 1.5 mL. During the extraction process, CO₂ was chosen as a buffer to balance the pH of the solution as it is cheaper and easily available compared to other solution buffers. Moreover, CO₂ will not introduce other cations, which may interfere with the ICP testing, therefore, can reflect the actual results of the extraction process for every cation. After the 3rd extraction stage, the solution in the enrichment was taken out. And then added the Na₃PO₄ into it to get the final solid production Li₃PO₄.

The Li/Mg selectivity ($S_{Li/Mg}$) and Li/Na selectivity ($S_{Li/Na}$) for each stage were calculated by the following Eqs. (3) and (4):

$$S_{Li/Mg} = \left(\frac{C_{Li,i}}{C_{Li,sw}} \right) / \left(\frac{C_{Mg,i}}{C_{Mg,sw}} \right) \quad (3)$$

$$S_{Li/Na} = \left(\frac{C_{Li,i}}{C_{Li,sw}} \right) / \left(\frac{C_{Na,i}}{C_{Na,sw}} \right) \quad (4)$$

where $C_{Li,i}$, $C_{Mg,i}$, $C_{Na,i}$, $C_{Li,sw}$, $C_{Mg,sw}$, and $C_{Na,sw}$ are the mole concentrations of Li⁺, Mg²⁺, and Na⁺ in the i^{th} enriched solution and seawater, respectively.

To identify the validation of the selectivity of the LAGP membrane, a constant voltage (2.5 V) was supplied by a potentiostat to drive the extraction process instead of a PEC cell and pure LiCl solution (50 mL, 1 ppm Li⁺) was prepared to replace the seawater in the feed chamber with other conditions remaining fixed.

The economic value produced by the PEC extraction system was calculated as follows:

As the solar to lithium efficiency (η_{STLi}) is 0.15 mg kJ⁻¹ and assuming there is 8 h 1-sun illumination per day, the mass of lithium per m² per day can be calculated:

$$m_{Li} = P_{in} \times time \times \eta_{STLi} = 1kWm^{-2} \times (8 \times 3600)s \times 0.15mgkJ^{-1} = 4.3g$$

In addition, the mass percentage of Li in Li₂CO₃ is 18.79%, Therefore, ~22.8 kg Li₂CO₃ can be obtained per m² per day. Finally, the price of Li₂CO₃ in April 2022 is around US\$75 per kg. The total economic value produced by our system is as high as ~US\$ 1.7 m⁻² per day.

Photoelectrochemical and electrochemical characterization

The Ru-Ir-TiO_x dark electrodes and III-V-based photoanodes were characterized in a three-electrode configuration: the (photo)anode as the working electrode, an Ag/AgCl/3 M KCl (Metrohm AG) reference, and a platinum coil counter electrode. LSV was typically conducted at a scan rate of 2 mV s⁻¹. The potentials were converted to RHE by using the following Nernst equation:

$$E_{RHE}(V) = E_{Ag/AgCl}(V) + E_{Ag/AgCl}^0(V) + 0.0591 \times pH \quad (5)$$

$E_{(Ag/AgCl)}$ is the experimentally measured potential, and $E_{(Ag/AgCl)}^0$ is the standard potential at 25 °C.

Microstructure characterization

Morphology of samples was observed using SEM (FEI© Magellan) with a beam energy of 5 kV. In addition, XRD patterns were recorded at 25 °C using a Bruker D8 Advance powder diffractometer (German Bruker) equipped with a LynxEye detector and a Cu source. ICP-OES was carried out using ICP-OES-Agilent 5110 equipment with an autosampler. Mixed standards (Li^+ , Na^+ , K^+ , Mg^{2+} , and Ca^{2+}) with concentrations of 0.1–100 ppm (4 points per magnitude) were calibrated. Liquid samples were diluted using 1% aqueous nitric acid to obtain the required concentration range.

Abbreviations

Li	Lithium
PEC	Photoelectrochemical
3J	Triple-junction
HAADF-STEM	High-angle annular dark-field scanning transmission electron microscopy
FF	Fill factor
EQE	External quantum efficiency
LAGP	$\text{Li}_{1.5}\text{Al}_{0.5}\text{Ge}_{1.5}(\text{PO}_4)_3$
XRD	X-ray diffraction
CIER	Chlorine evolution reaction
η_{STLi}	Solar-to-Li extraction efficiency
η_{STH}	Solar-to-hydrogen efficiency

Supplementary Information

The online version contains supplementary material available at <https://doi.org/10.1186/s43074-023-00100-9>.

Additional file 1: Figure S1. Schematic diagram of (a) the typical monofacial PEC design and the light loss mechanism, in which all functionalities, such as the surface protection layer and electrocatalyst, are integrated on top of the light-harvesting side, whereas the bottom side is only used for the electrical connection; (b) the light-decoupled device, in which the light-harvesting component is decoupled from the protection and electrocatalysis functions. **Figure S2.** (a) SEM image of the LAGP powder prepared via the solid-state reaction method. (b) SEM image of the cross-section of the LAGP membrane. **Figure S3.** (a) Crystal structure of LAGP (the blue and pink polyhedrons are the GeO_6 and PO_4 groups, respectively; the black balls are the Li atoms at 36f Wyckoff sites; the yellow balls are the 6b Wyckoff sites for potential Li atoms; oxygen atoms (not shown) are located on the tops of the polyhedrons). (b) Illustration of the “lantern” substructures and triangular bottlenecks. **Figure S4.** XRD patterns of the LAGP powder, and LAGP membrane before and after extraction process. **Figure S5.** The chronoamperometric curve of extraction of 1 ppm Li^+ simulation solution at 2.5 V for 2h. The inset shows the schematic diagram of the extraction process and the ICP results of the Li^+ concentration before (cfeed, before) and after (cfeed, after) extraction in the feed chamber and the final amount (enrichment) in the enrichment chamber. **Figure S6.** SEM image of the LAGP membrane before (a) and after (b) Li extraction process. **Figure S7.** Literature comparison of the measured photocurrent density (X-axis) vs. stability time (Y-axis) of photoelectrodes used in the seawater [2–7]. **Figure S8.** The averaged current density of the whole process (J) and the corresponding solar-to-hydrogen efficiency (η_{STH}) for each stage. **Figure S9.** (a) and (b) SEM images of the Ru-Ir-TiOx catalyst layer on the Ti plate. (c) SEM images of the cross-section of the Ru-Ir-TiOx electrode. **Table S1.** The separation performance of PEC Li extraction system from seawater. **Table S2.** Comparison of Li extraction performance from aqueous resource.

Acknowledgements

We acknowledge the financial support from City University of Hong Kong and King Abdullah University of Science and Technology.

Authors' contributions

Z. X. Li, Z. Li and H. Huang, contributed equally. J.-H. He, K.-W. Huang and Z. P. Lai conceived the idea and supervised the project. Z. X. Li, H. Huang fabricated the PEC device. Z. Li prepared the LAGP membrane. Z. X. Li, Z. Li, and H. Huang conducted the lithium enrichment experiments, analyzed the data, and wrote the manuscript. Y. D. Yao, and Z. Ye performed the electrochemical test. B. Khan conducted the ICP and PEC measurements. All authors revised and commented on the writing of the manuscript.

Funding

This work was financially supported by the City University of Hong Kong funding (No. 9380107).

Availability of data and materials

The datasets analyzed and generated during the current study are included in the paper and its Supplementary Information.

Declarations

Ethics approval and consent to participate

Not applicable.

Consent for publication

Not applicable.

Competing interests

All authors declare no competing interests.

Received: 10 January 2023 Revised: 19 May 2023 Accepted: 19 June 2023

Published online: 10 July 2023

References

1. Zhao J, Hong M, Ju Z, Yan X, Gai Y, Liang Z. Durable lithium metal anodes enabled by interfacial layers based on mechanically interlocked networks capable of energy dissipation. *Angew Chem Int Ed Engl.* 2022;61:e202214386.
2. Yue X, Zhang J, Dong Y, Chen Y, Shi Z, Xu X, et al. Reversible Li plating on graphite anodes through electrolyte engineering for fast-charging batteries. *Angew Chem Int Ed Engl.* 2023;62:e202302285.
3. YaghoobnejadAsl H, Manthiram A. Toward sustainable batteries. *Nat Sustain.* 2020;4:379–80.
4. Zhu X, Meng F, Zhang Q, Xue L, Zhu H, Lan S, et al. LiMnO₂ cathode stabilized by interfacial orbital ordering for sustainable lithium-ion batteries. *Nat Sustain.* 2020;4:392–401.
5. U.S. Geological Survey, Lithium. In: Mineral commodity summaries 2022. U.S. Geological Survey. 2022. <https://doi.org/10.3133/mcs2022>. Accessed 6 July 2022.
6. Yang S, Zhang F, Ding H, He P, Zhou H. Lithium metal extraction from seawater. *Joule.* 2018;2:1648–51.
7. Wanger TC. The Lithium future-resources, recycling, and the environment. *Conserv Lett.* 2011;4:202–6.
8. Tang L, Huang S, Wang Y, Liang D, Li Y, Li J, et al. Highly efficient, stable, and recyclable hydrogen manganese oxide/cellulose film for the extraction of lithium from seawater. *ACS Appl Mater Interfaces.* 2020;12:9775–81.
9. Hong HJ, Ryu T, Park IS, Kim M, Shin J, Kim BG, et al. Highly porous and surface-expanded spinel hydrogen manganese oxide (HMO)/Al₂O₃ composite for effective lithium (Li) recovery from seawater. *Chem Eng J.* 2018;337:455–61.
10. Liu C, Li Y, Lin D, Hsu PC, Liu B, Yan G, et al. Lithium extraction from seawater through pulsed electrochemical intercalation. *Joule.* 2020;4:1459–69.
11. Yu J, Fang D, Zhang H, Leong ZY, Zhang J, Li X, et al. Ocean mining: a fluidic electrochemical route for lithium extraction from seawater. *ACS Mater Lett.* 2020;2:1662–8.
12. Ryu T, Haldorai Y, Rengaraj A, Shin J, Hong H-J, Lee G-W, et al. Recovery of lithium ions from seawater using a continuous flow adsorption column packed with granulated chitosan-lithium manganese oxide. *Ind Eng Chem Res.* 2016;55:7218–25.
13. Kim JH, Hansora D, Sharma P, Jang JW, Lee JS. Toward practical solar hydrogen production - an artificial photosynthetic leaf-to-farm challenge. *Chem Soc Rev.* 2019;48:1908–71.
14. Kang D, Young JL, Lim H, Klein WE, Chen H, Xi YZ, et al. Printed assemblies of GaAs photoelectrodes with decoupled optical and reactive interfaces for unassisted solar water splitting. *Nat Energy.* 2017;2:17043.
15. Sathre R, Greenblatt JB, Walczak K, Sharp ID, Stevens JC, Ager JW, et al. Opportunities to improve the net energy performance of photoelectrochemical water-splitting technology. *Energy Environ Sci.* 2016;9:803–19.
16. Landman A, Halabi R, Dias P, Dotan H, Mehlmann A, Shter GE, et al. Decoupled photoelectrochemical water splitting system for centralized hydrogen production. *Joule.* 2020;4:448–71.
17. Walter MG, Warren EL, McKone JR, Boettcher SW, Mi Q, Santori EA, et al. Solar water splitting cells. *Chem Rev.* 2010;110:6446–73.
18. Peerakiatkhajohn P, Yun J-H, Wang S, Wang L. Review of recent progress in unassisted photoelectrochemical water splitting: from material modification to configuration design. *J Photon Energy.* 2016;7:012006.
19. Pinaud BA, Benck JD, Seitz LC, Forman AJ, Chen Z, Deutsch TG, et al. Technical and economic feasibility of centralized facilities for solar hydrogen production via photocatalysis and photoelectrochemistry. *Energy Environ Sci.* 2013;6:1983–2002.
20. Shaner MR, Atwater HA, Lewis NS, McFarland EW. A comparative technoeconomic analysis of renewable hydrogen production using solar energy. *Energy Environ Sci.* 2016;9:2354–71.
21. Grimm A, de Jong WA, Kramer GJ. Renewable hydrogen production: a techno-economic comparison of photoelectrochemical cells and photovoltaic-electrolysis. *Int J Hydrogen Energy.* 2020;45:22545–55.
22. Ye S, Shi W, Liu Y, Li D, Yin H, Chi H, et al. Unassisted photoelectrochemical cell with multimediator modulation for solar water splitting exceeding 4% solar-to-hydrogen efficiency. *J Am Chem Soc.* 2021;143:12499–508.
23. Zhang Y, Lv H, Zhang Z, Wang L, Wu X, Xu H. Stable unbiased photo-electrochemical overall water splitting exceeding 3% efficiency via covalent triazine framework/metal oxide hybrid photoelectrodes. *Adv Mater.* 2021;33:e2008264.
24. Yang W, Kim JH, Hutter OS, Phillips LJ, Tan J, Park J, et al. Benchmark performance of low-cost Sb₂Se₃ photocathodes for unassisted solar overall water splitting. *Nat Commun.* 2020;11:861.
25. Li Z, Li C, Liu X, Cao L, Li P, Wei R, et al. Continuous electrical pumping membrane process for seawater lithium mining. *Energy Environ Sci.* 2021;14:3152–9.
26. Hoshino T. Innovative lithium recovery technique from seawater by using world-first dialysis with a lithium ionic superconductor. *Desalination.* 2015;359:59–63.
27. Zhang F, Yang S, Du Y, Li C, Bao J, He P, et al. A low-cost anodic catalyst of transition metal oxides for lithium extraction from seawater. *Chem Comm.* 2020;56:6396–9.

28. Zhao X, Zhang H, Yuan Y, Ren Y, Wang N. Ultra-fast and stable extraction of Li metal from seawater. *Chem Comm.* 2020;56:1577–80.
29. Li Y, Wang R, Li H, Wei X, Feng J, Liu K, et al. Efficient and stable photoelectrochemical seawater splitting with $\text{TiO}_2/\text{g-C}_3\text{N}_4$ nanorod arrays decorated by Co-Pi. *J Phys Chem C.* 2015;119:20283–92.
30. Liu J, Xu SM, Li Y, Zhang R, Shao M. Facet engineering of WO_3 arrays toward highly efficient and stable photoelectrochemical hydrogen generation from natural seawater. *Appl Catal B.* 2020;264:118540.
31. She X, Ma G, Zhang L, Jiao S, Cheng G, Zhang Z. Floc-like CNTs jointed with $\text{Bi}_x\text{Fe}_{1-x}\text{VO}_4$ nanoparticles for high efficient and stable photoelectrochemical seawater splitting. *J Alloys Compd.* 2022;893:162146.
32. Li Y, Feng J, Li H, Wei X, Wang R, Zhou A. Photoelectrochemical splitting of natural seawater with $\alpha\text{-Fe}_2\text{O}_3/\text{WO}_3$ nanorod arrays. *Int J Hydrogen Energy.* 2016;41:4096–105.
33. Guo X, Liu X, Wang L. NiMoO_x as a highly protective layer against photocorrosion for solar seawater splitting. *J Mater Chem A.* 2022;10:1270–7.
34. Luo W, Yang Z, Li Z, Zhang J, Liu J, Zhao Z, et al. Solar hydrogen generation from seawater with a modified BiVO_4 photoanode. *Energy Environ Sci.* 2011;4:4046–51.
35. Verlage E, Hu S, Liu R, Jones RJR, Sun K, Xiang CX, et al. A monolithically integrated, intrinsically safe, 10% efficient, solar-driven water-splitting system based on active, stable earth-abundant electrocatalysts in conjunction with tandem III-V light absorbers protected by amorphous TiO_2 films. *Energy Environ Sci.* 2015;8:3166–72.
36. Varadhan P, Fu HC, Kao YC, Horng RH, He JH. An efficient and stable photoelectrochemical system with 9% solar-to-hydrogen conversion efficiency via InGaP/GaAs double junction. *Nat Commun.* 2019;10:5282.
37. Li D, Yang K, Lian J, Yan J, Liu S. Powering the world with solar fuels from photoelectrochemical CO_2 reduction: basic principles and recent advances. *Adv Energy Mater.* 2022;12:2201070.
38. Cheng W-H, Richter MH, May MM, Ohlmann J, Lackner D, Dimroth F, et al. Monolithic photoelectrochemical device for direct water splitting with 19% efficiency. *ACS Energy Lett.* 2018;3:1795–800.
39. Jia K, Ma J, Wang J, Liang Z, Ji G, Piao Z, et al. Long-life regenerated LiFePO_4 from spent cathode by elevating the d-Band center of Fe. *Adv Mater.* 2023;35:e2208034.
40. Ji G, Wang J, Liang Z, Jia K, Ma J, Zhuang Z, et al. Direct regeneration of degraded lithium-ion battery cathodes with a multifunctional organic lithium salt. *Nat Commun.* 2023;14:584.
41. Wang J, Ma J, Jia K, Liang Z, Ji G, Zhao Y, et al. Efficient extraction of lithium from anode for direct regeneration of cathode materials of spent Li-ion batteries. *ACS Energy Lett.* 2022;7:2816–24.
42. Ma J, Wang J, Jia K, Liang Z, Ji G, Zhuang Z, et al. Adaptable eutectic salt for the direct recycling of highly degraded layer cathodes. *J Am Chem Soc.* 2022;144:20306–14.
43. Hoseinie SM, Ashrafzadeh F, Maddahi MH. A comparative investigation of the corrosion behavior of $\text{RuO}_2\text{-IrO}_2\text{-TiO}_2$ coated titanium anodes in chloride solutions. *J Electrochem Soc.* 2010;157:E50–6.
44. Moon C, Seger B, Vesborg PCK, Hansen O, Chorkendorff I. Wireless photoelectrochemical water splitting using triple-junction solar cell protected by TiO_2 . *Cell Rep Phys Sci.* 2020;1:100261.

Publisher's Note

Springer Nature remains neutral with regard to jurisdictional claims in published maps and institutional affiliations.

Submit your manuscript to a SpringerOpen[®] journal and benefit from:

- Convenient online submission
- Rigorous peer review
- Open access: articles freely available online
- High visibility within the field
- Retaining the copyright to your article

Submit your next manuscript at ► [springeropen.com](https://www.springeropen.com)
